Journal of Hydroinformatics

Journal of Hydroinformatics Vol 24 No 2, 243 doi: 10.2166/hydro.2022.031

The effect of triangular prismatic elements on the hydraulic performance of stepped spillways in the skimming flow regime: an experimental study and numerical modeling

Kiyoumars Roushangar[a,b], Samira Akhgar[a,*] and Saman Shahnazi[a]

[a] Department of Water Resources Engineering, Faculty of Civil Engineering, University of Tabriz, Tabriz, Iran
[b] Center of Excellence in Hydroinformatics, University of Tabriz, Tabriz, Iran
*Corresponding author. E-mail: samira.akhgar66@yahoo.com

ABSTRACT

The stepped spillway is a cost-effective hydraulic structure to dissipate the energy of large water flow over the spillway of a dam. In this study, the focus was placed on the effects of triangular prismatic elements (TPEs) on the hydraulic performance of a stepped spillway. Nine stepped spillway models were experimentally and numerically investigated with different shapes and layouts of TPEs. To adopt a proper turbulent model, RNG k-ε and standard k-ε models were utilized. The computational model results satisfactorily simulated the complex flow over the stepped spillway of experiment cases, including velocity distributions and pressure profiles on the step surfaces. The results indicated that the installation of TPEs on stepped spillways can be an effective way to reduce cavitation effects. Installing TPEs on stepped spillways increased the energy dissipation rate up to 54%. The performance of stepped spillways was improved when TPEs were spaced more closely together. Furthermore, the relationships between the roughness coefficient (f) and the ratio of the critical depth to the step roughness (yc/k) were obtained with high accuracy using the experimental data.

Key words: energy dissipation, Flow-3D, roughness coefficient, stepped spillway, triangular prismatic elements

HIGHLIGHTS

- The Flow-3D model was applied to examine the effects of triangular prismatic elements (TPEs) on the hydraulic performance and energy dissipation of stepped spillways.
- Two types of TPEs with different spacing were experimentally investigated for varied flow rates.
- Stepped spillways with TPEs are more efficient in terms of energy dissipation.

INTRODUCTION

Spillways are widely used for passing excess flow and reducing the risk of dam failure (Roushangar *et al.* 2019). The kinetic energy at the spillway toe of large dams is such that it can lead to scouring (Bakhtyar & Barry 2009). Stepped spillways are efficient energy dissipaters that reduce construction dimensions and the cost of the downstream stilling structures. The steps act as roughness elements to reduce the kinetic energy of flow. Moreover, stepped spillways are effective hydraulic structures for aeration in water flow owing to their intense turbulent mixing of large quantities of air bubbles (Toombes & Chanson 2000). Spillway flows are classified into three major regimes with regard to discharge rates. For a range of small discharges, a nappe flow regime is dominant, and on the other hand, transient flow for intermediate discharge rates and skimming flow for high discharge rates can be observed. During the last three decades, physical models of standard stepped spillways (without roughness elements) have been developed with a focus on the energy dissipation (Chamani & Rajaratnam 1994; Chanson 1994; Azhdary Moghaddam 1997; Boes & Hager 2003; Kavian Pour & Masoumi 2008). Among them, Barani *et al.* (2005) highlighted the significant role of the step shape on the energy dissipation of spillways. Consequently, V-shaped (Peng *et al.* 2019) and circular crested stepped spillways (Parsaie & Haghiabi 2019) were introduced to achieve better energy dissipation. Detailed studies on energy dissipation of these modified stepped spillways indicated noticeable advantages in comparison to conventional stepped spillways. Wüthrich & Chanson (2014) performed experiments to address detailed flow properties and energy dissipation over the normal and gabion-stepped spillways. Their findings demonstrated lower energy dissipation rates over the gabion-stepped spillways in comparison with smooth, impermeable steps. Sarkardeh *et al.* (2015) employed a

physical model of the stepped spillway to modify the zone where the stepped chute profile and the ogee spillway crest are joined together. The results obtained from studies of Torabi *et al.* (2018) *in situ* indicated that the roughness of the steps may enhance the performance of the spillway in terms of energy dissipation by 15–20% compared to the stepped spillway without step roughness. Benefiting from fast-growing computing power, various models have been employed in recent years in the domain of numerical models. Therefore, using computational fluid dynamics (CFD) to study the effect of the number of steps, step height, sizes of step, and spillway slope on the amount of energy dissipation have been the goal of several researchers (Abbasi & Kamanbedast 2012; Attarian *et al.* 2014; Shahheydari *et al.* 2015; Tabari & Tavakoli 2016). Moreover, step configurations have become a matter of concern for an optimal design adapted to varied hydraulic conditions due to its substantial role in the improvement of energy dissipation and aeration efficiency. Hekmatzadeh *et al.* (2018) demonstrated more efficiency of the flat stepped spillway in comparison to the pooled stepped spillway if the spillway slope exceeds 14°. Li *et al.* (2019) provided numerical insight into the hydraulic characteristics of V-shaped spillways with several step layouts. Arjenaki & Sanayei (2020) carried out a numerical analysis to investigate the effects of different types of step geometries on the energy dissipation rate of stepped spillways. The results showed that some step geometries with rectangular blocks can increase energy dissipation rates by as much as two times. In another numerical investigation into the hydraulic characteristics of the air–water flows over a stepped spillway, more recently, Li *et al.* (2020) found that chamfering the step edges led to slight improvements in the total energy dissipation. Moghadam *et al.* (2020) numerically investigated the energy dissipation capability of block barriers with various geometries in stepped spillways. They arrived at the fact that the blocks with the ratios $H_b/h = L_b/B$ (block height to step height and block length to step length) equal to 0.3 and 0.5 applied the most effects on dissipation.

Although there has been significant experimental and numerical research associated with stepped spillways, there is a lack of comprehensive research on the effects of roughness elements on stepped spillway performance. Therefore, the main goal of the present study is to gain a greater understanding of the effects of triangular prismatic elements (TPEs) on the complex skimming flow properties over the stepped spillways. To this end, several forms of TPEs are developed, and the impacts of changing the prismatic layout and the discharge rate on the variations of the velocity and pressure on the steps, Darcy–Weisbach roughness coefficient (f), water level, and consequently, downstream energy dissipation are analyzed using the Flow-3D CFD package.

Physical and experimental characteristics

The experimental parts of this research were conducted in the Hydraulic Laboratory, Department of Civil Engineering, University of Tabriz, Iran. The experimental facility is comprised of a smooth, toughened glass-sided and galvanized steel bottomed flume that is 10 m long, 0.5 m wide, and 0.8 m deep. Rolling point gauge instrumentation, with ± 0.1 mm measurement accuracy, was used in order to measure the water height above the weir and at different locations upstream of the stepped spillway (Figure 1). The channel was equipped with two grid walls and wave suppressors as upstream stilling structures to achieve the steady approach flow. The geometric model of the standard form of the stepped spillway is 50 cm wide with six steps. The total height of the fabricated spillway was adjusted to 60 cm ($H = 60$ cm), where the step height of the model is 10 cm ($W = h = 10$ cm). The stepped spillway model was installed at 4 m downstream of where the water enters the headbox. The discharge was measured by means of a magnetic flow meter installed in the supply line with an accuracy of 5%. The water depth was measured through a gauge by a ± 0.1 mm precision at the end of the hydraulic jump. In high

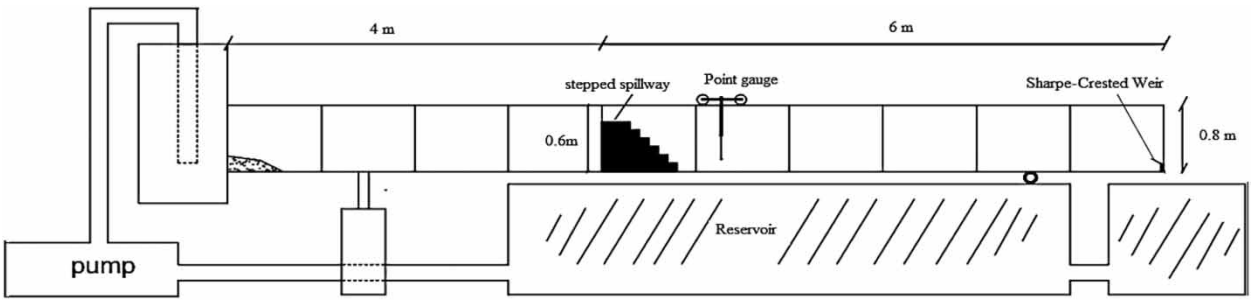

Figure 1 | General schematics of laboratory flume facilities.

discharges, in contrast to low discharge, the water depth varies across the flume due to the flow turbulence which makes its evaluation difficult. When it is the case, the sequent depth of the hydraulic jump (y_2) is determined, and with the help of hydraulic equations, the primary depth is obtained. Velocities were measured with an ultrasonic ADV device (vecterino model with an accuracy of 200 MHz). Four different layouts of TPEs were investigated for discharges ranging from 10 to 60 liters/second, and consequently, a total of 25 experiments were performed, as shown in Figure 2. Samples of laboratory data for the common stepped spillway and stepped spillway with TPEs are given in Table 1.

NUMERICAL FLOW SIMULATION

The full geometry of the three-dimensional stepped spillway with the TPEs is prepared through 'solid modeler,' computer-aided design (CAD) files. The developed framework is embedded in FLOW-3D® as a high potential CFD code to simulate the effect of TPEs on the flow pattern over the stepped spillway. The geometry and layout of the TPEs are illustrated in Figure 3. Two different TPEs were used:

Type A: A triangle with a base equal to 0.2 times the width of the channel

Type B: A triangle with a base equal to 0.3 times the width of the channel

The height of the triangles was fixed for both types of TPEs (100 mm). Four different spacings for each element were numerically simulated for varied flow rates ranging from 10 to 60 liters/second. As a result, a total of nine different layouts, including the standard stepped spillway, were investigated in the present study.

Flow-3D utilizes a Reynolds-averaged Navier–Stokes (RANS) approach, numerically discretized through the use of the finite volume/-finite difference method in a Cartesian, staggered grid system. Average values of the flow parameter for each computational cell are calculated at discrete times through a staggered grid method. The governing equations can be outlined as follows:

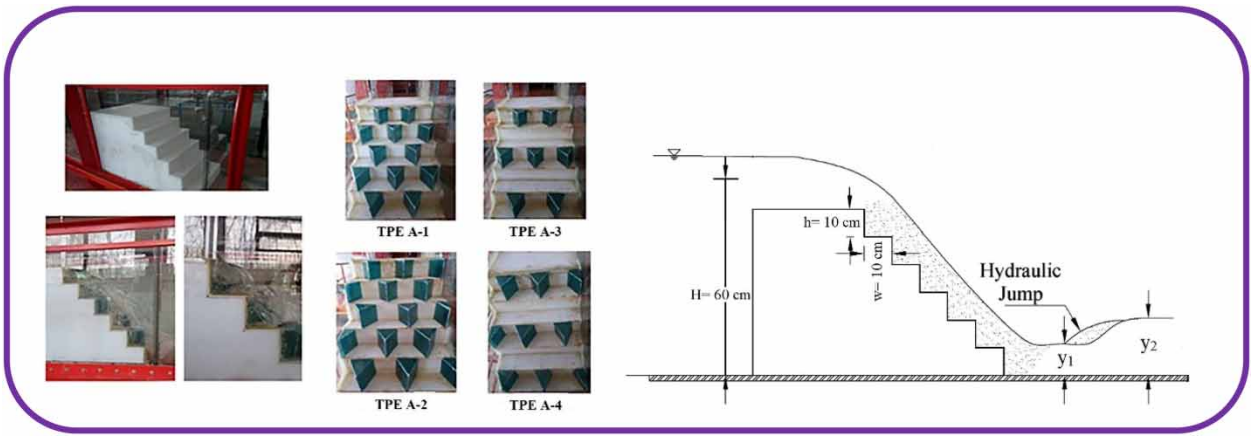

Figure 2 | Different layouts of the selected TPE in the experimental study (y_1 and y_2 are initial, and sequent depths of hydraulic jump).

Table 1 | Samples of laboratory data for the standard stepped spillway and TPE A-4

Stepped spillway type	Q (liters/second)	Reynolds number	Head water (cm)	Tail water (cm)	Y_c (cm)
Standard stepped spillway	20	16.3×10^5	7.4	18	5.5
	30	17×10^5	9.6	21	7.1
	40	18.2×10^5	11	22	8.7
	50	20.1×10^5	13	25	10.1
	60	21.3×10^5	14.6	29	11.3
TPE A-4	20	13.7×10^5	7.4	14	5.5
	30	14.9×10^5	9.6	18	7.1
	40	15.1×10^5	11	21	8.7
	50	15.4×10^5	13	23	10.1
	60	15.8×10^5	14.6	26	11.3

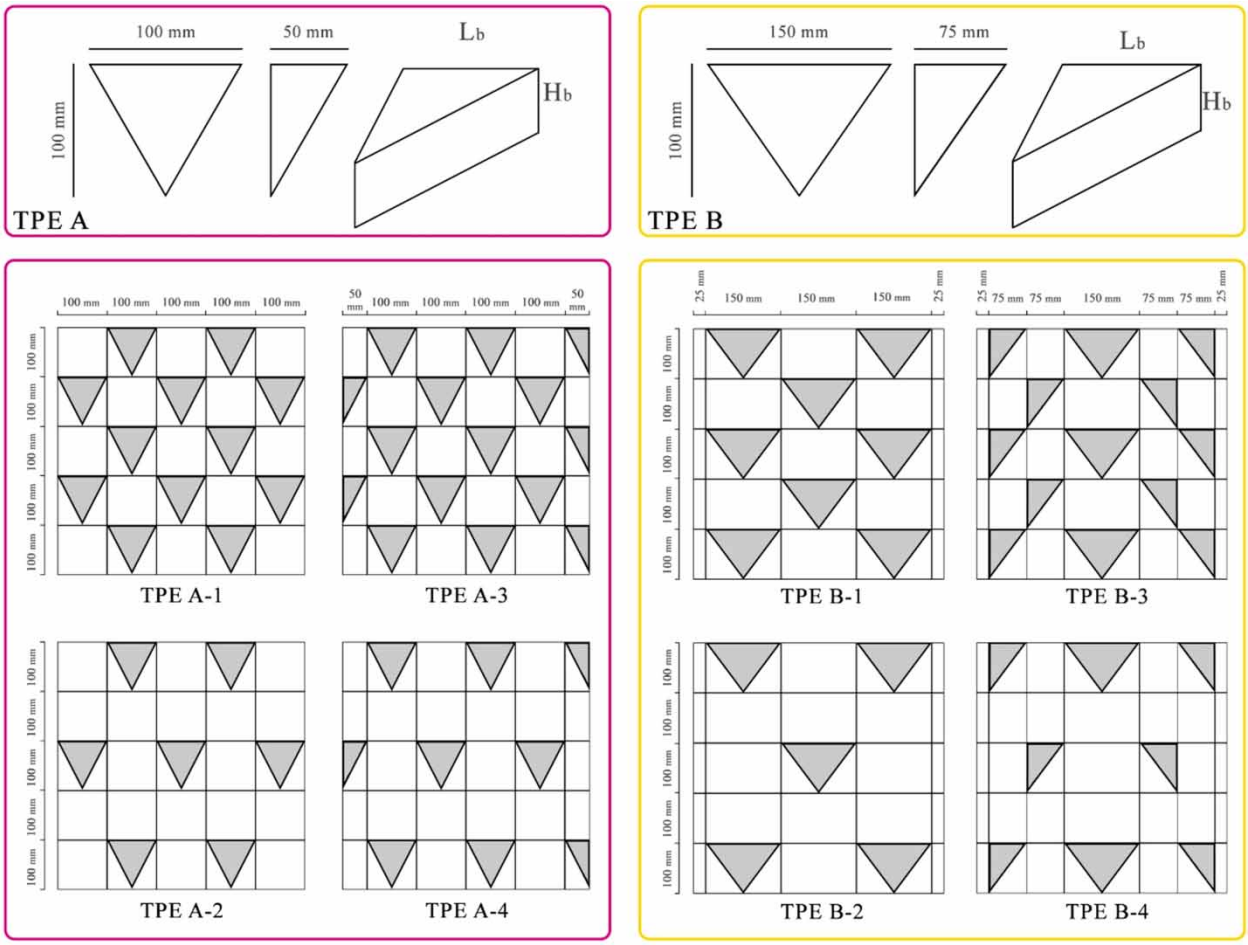

Figure 3 | Geometry and alignment of TPE in the numerical study.

Continuity equation:

$$\frac{\partial}{\partial x}(uA_x) + R\frac{\partial}{\partial y}(vA_y) + \frac{\partial}{\partial z}(wA_z) + \xi\frac{uA_x}{x} = \frac{\text{RSOR}}{\rho} \tag{1}$$

where ρ stands as the density of the fluid, u, v, and w, respectively, are the velocity in x, y, and z directions in Cartesian coordinates, A_x, A_y, and A_z are defined as the differential area in these directions, and RSOR is known as the mass source. Parameters of R and ξ are considered to be 1 and 0, respectively, in the Cartesian coordinate.

Momentum equations:

$$\frac{\partial u}{\partial t} + \frac{1}{V_F}\left\{uA_x\frac{\partial u}{\partial x} + vA_yR\frac{\partial u}{\partial y} + wA_z\frac{\partial u}{\partial z}\right\} - \xi\frac{A_yv^2}{xV_F} = -\frac{1}{\rho}\frac{\partial p}{\partial x} + G_x + f_x - b_x - \frac{\text{RSOR}}{\rho V_F}u \tag{2}$$

$$\frac{\partial v}{\partial t} + \frac{1}{V_F}\left\{uA_x\frac{\partial v}{\partial x} + vA_yR\frac{\partial v}{\partial y} + wA_z\frac{\partial v}{\partial z}\right\} - \xi\frac{A_yuv}{xV_F} = -\frac{1}{\rho}\frac{\partial p}{\partial y} + G_y + f_y - b_y - \frac{\text{RSOR}}{\rho V_F}y \tag{3}$$

$$\frac{\partial w}{\partial t} + \frac{1}{V_F}\left\{uA_x\frac{\partial w}{\partial x} + vA_yR\frac{\partial w}{\partial y} + wA_z\frac{\partial w}{\partial z}\right\} = -\frac{1}{\rho}\frac{\partial p}{\partial_{zx}} + G_z + f_z - b_z - \frac{\text{RSOR}}{\rho V_F}w \tag{4}$$

where VF is the fraction of fluid, G_x, G_y, and G_z are the body acceleration, f_x, f_y, and f_z are the viscous dissipations, and b_x, b_y, and b_z are the flow losses in porous media. The multiphase air-water interface was tracked using the well-known volume of fluid (VOF) method.

The entrainment rate coefficient was defined as a positive value and defaulted to 0.5, which is suitable for most cases. The variable density model with density transport is activated in Physics > Density evaluation to take into account the changes of fluid density due to entrained air. In this case, the value for air density (0.0012) in the air entrainment model panel was inputted. In addition to the variable density model, the drift-flux model is activated to model the fluid/air mixture as a two-phase flow. In this case, the air bubbles can move within fluid due to the difference in their densities drift flux. They allow gas to escape at the free surface check box, in which the entrained air could also escape back into the atmosphere.

For accurate and efficient results, convergence criteria are given as follows:

1. The size ratio between adjacent cells should be as close to unity as possible, and not exceed 1.25.
2. Cell aspect ratios should be as close to unity as possible, and not exceed 3.0. (Morovati *et al.* 2016). Simulation boundary features for inlet, outlet, wall, free surface, and mesh information are listed in Table 2.

In this study, the non-uniform (inflated) Cartesian mesh is used, fixed points or mesh plans are defined both in the direction of flow (X) and perpendicular to it (Z). The total number of cells is specified (14 million cells). That number is divided among the checked directions, taking into account the length of each direction, to give the most uniform mesh possible in those directions. Also, a uniform cell size is specified; the cell size will be set to the closest value that divides the domain evenly, for each checked direction. The layout of the numerical model and the schematic of the size of non-uniform meshes for high-precision inspection on downstream steps are depicted in Figure 4.

VALIDATION MODEL

Since numerous turbulence closures have been developed and incorporated in Flow-3D, two types, as well as the k-ε model (Harlow & Nakayama 1968) and renormalized-group (RNG) model (Yakhot & Orszag 1986; Yakhot & Smith 1992), were adopted for the numerical simulation of flow patterns over the stepped spillway. Felder *et al.*'s (2012) experimental data have been used to verify the numerical model and to investigate turbulence models. By comparison of the outcomes of the turbulence model with the experimental data, the best numerical model was determined. It is necessary to validate the reliability of the selected RNG turbulence model before further analysis. Therefore, experimental data with a flow discharge of 60 liters/second were used to verify the numerical results by comparing the velocity distribution on steps 4, 5, and 6, as shown in Figure 5. Moreover, the mean relative error (MRE) between the experimental and numerical distribution of velocity on steps 4, 5, and 6 is listed in Table 3. It can be noticed from this figure that, at most locations, the simulated results of velocity distribution were fairly consistent with those of experimental tests. The maximum values of the MRE for steps 4, 5, and 6 were 8.57, 10.72, and 11.18%, respectively, indicating that the numerical simulations achieved the best agreement with the experimental data in step 4. Analysis of the obtained velocity distributions from employed turbulence models shows that although the k-ε model has better performance near the water surface of step 5, the RNG turbulent model shows better performance for modeling the velocity distribution.

RESULTS AND DISCUSSIONS

This study presents a numerical solution to investigate the effects of TPEs on the flow pattern of stepped spillways. In high discharges, the flow turbulence leads to variations in water depth across the flume, which makes its assessment complicated. In this case, the velocity at the toe of the spillway was indirectly determined through the sequent depth of the hydraulic jump and by using the mass and momentum conservation equations. The values of sequent depth (y_2) are plotted against the unit discharges in Figure 6 for different types of stepped spillways. It can be seen that, in comparison with a standard stepped spillway, both types of TPEs can considerably reduce the sequent depth. Variations of the sequent depth for stepped spillways with TPEs are summed up in Table 4. Models A-3, A-1, A-4, and A-2 reduced the sequent depth by 30, 21, 14, and 13%, respectively, in comparison to the standard form of the stepped spillway, and showed better performance than TPEs of type B in terms of reducing the sequent depth.

As a consequence of the conservation of upstream and downstream energy, the ratio of the energy loss to the upstream energy is determined as the energy dissipation rate via the following equation:

$$\eta = \frac{\Delta E}{E_1} \times 100\% = \frac{E_1 - E_2}{E_1} \times 100\% \tag{5}$$

Table 2 | Boundary conditions for numerical modeling in Flow-3D

Direction	Total number of real cells	Minimum cell size	Maximum cell size	Maximum adjacent cell size ratio	Maximum aspect ratios		Total number of real cells	Mesh plane		Boundaries	
								Min.	Max.	Mix.	Max.
X	793	5	5.1	1.0014	*X-Y* direction	1.013	1,39,74,246	0.5	3.5	Volume of rate	Outflow
Y	99	5.1	5.1	1	*Y-Z* direction	1.019		0	0.5	Wall	Wall
Z	178	5	5.1	1.0002	*Z-X* direction	1.029		0	0.9	Wall	Symmetry

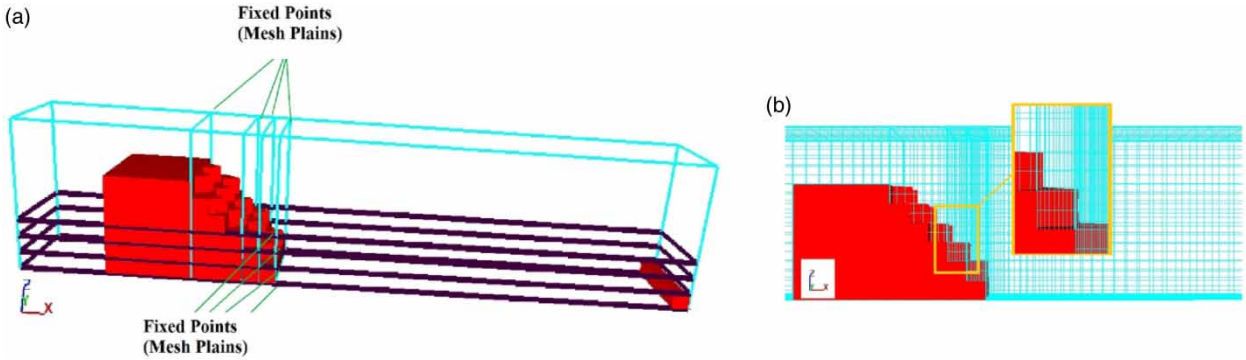

Figure 4 | The numerical model in the Flow-3D with mesh plains (a), the coarse, intermediate, and fine grid (b).

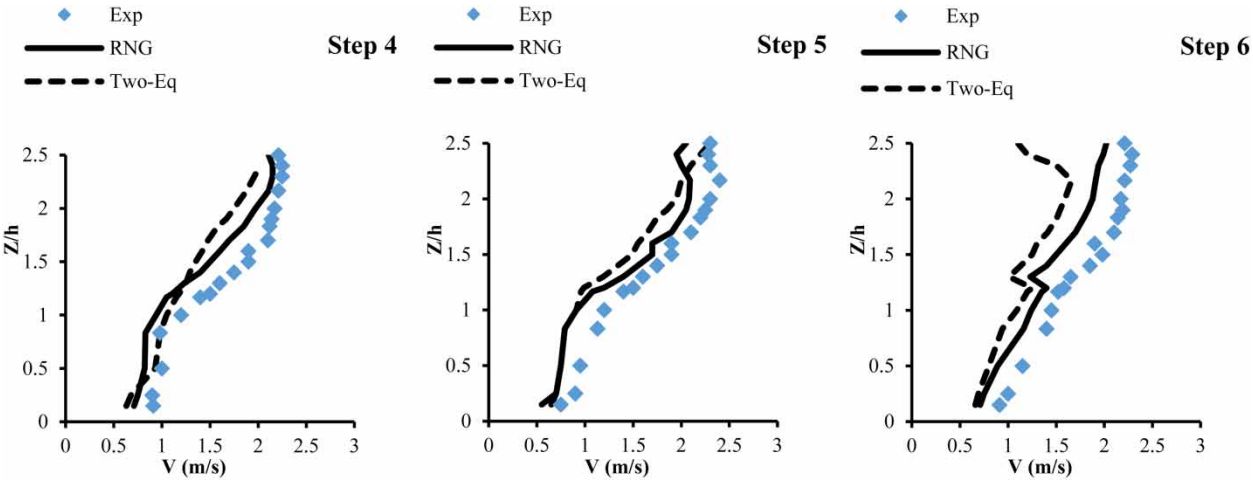

Figure 5 | Comparison of turbulence models in Flow-3D.

Table 3 | Percent average error for turbulence models

Turbulence models	Step 4	Step 5	Step 6
RNG	8.23	9.36	9.84
Two-equation (k-ε)	13.78	15.28	15.93

where E_1 and E_2 are the total energy in the beginning and end of the stepped section, respectively; $E_1 = \Delta h + V_1^2/(2g)$ and $E_2 = \Delta h + V_2^2/(2g)$, where Δh is the difference in the height between the two sections.

Figure 7 illustrates the numerical results pertaining to energy dissipation rates over the stepped spillways for different unit discharges. It can be seen that the energy dissipation rates in the standard form of the stepped spillway decreased with an increase in the unit discharge. On the other hand, for studied stepped spillways with various shapes and layouts of TPEs, the trends of energy dissipation were differently obtained. Generally, it is noticed that stepped spillways with TPEs are more efficient in terms of energy dissipation. In conformity with numerical results provided in Figures 6 and 7 and also in Table 3, it can be deduced that stepped spillways with TPEs of type A result in lower sequent depths and higher energy dissipation. Results indicated that closer spacing of the type A elements led to better performance. Therefore, models A-3, A-1, A-4, and A-2 demonstrated the best performance, respectively.

Pressure and velocity distributions

In this part of the study, the focus was placed on the variation of pressure and velocity on the horizontal and vertical surfaces of the stepped spillway with TPEs of type A. Since the pressure and velocity distributions varied along the cross-section in the

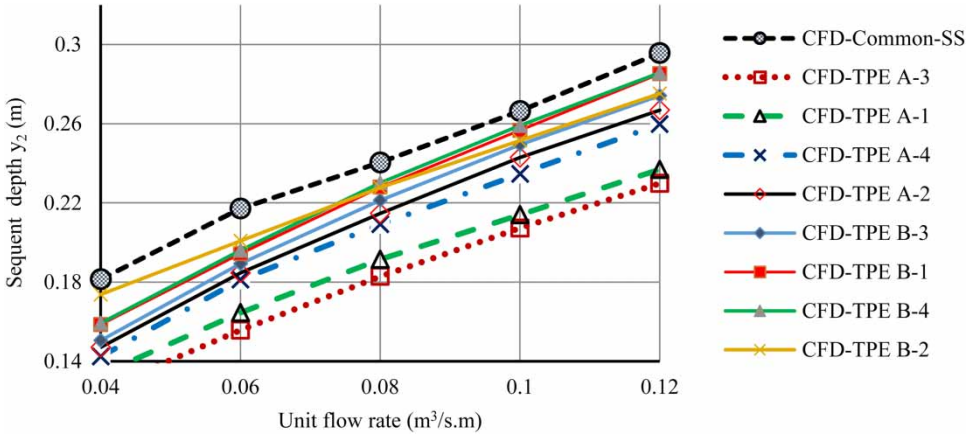

Figure 6 | Sequent water depths versus unit flow rate in standard stepped spillways and stepped spillways with triangular TPEs of types A and B.

Table 4 | Variation of sequent depth for the stepped spillway with prismatic-shaped elements of types A and B

Stepped spillway with TPEs	TPE A-1	TPE A-2	TPE A-3	TPE A-4	TPE B-1	TPE B-2	TPE B-3	TPE B-4
Variation of sequent depth (%)	21	13	30	14	10	6	11	7

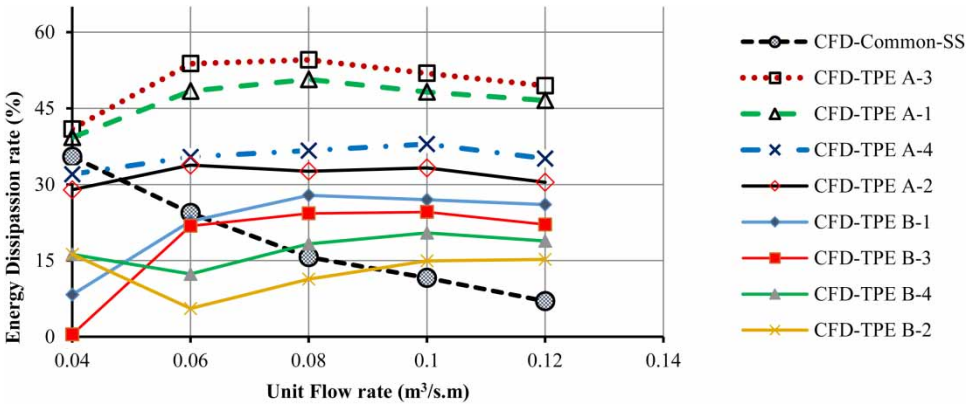

Figure 7 | Energy dissipation for the standard stepped spillway and the stepped spillway with TPEs.

stepped spillway, two measurement points were adopted in a uniform flow area on step 4. The positions of measurement points for models A-1 and A-2 were in $Y/B = 0.3$ (where the prismatic element is placed) and $Y/B = 0.5$ (where no TPEs are placed) and for models A-3 and A-4 were in $Y/B = 0.2$ (where the prismatic element is placed) and $Y/B = 0.4$ (where no TPEs are placed), as shown in Figure 8. In this figure, B represents the width of the channel (where $B = 0.5$ m), and Y represents the distance of the measurement points on the horizontal surface from the channel's wall.

Figure 9(a) highlights a comparison of the velocity distributions in the vertical surface of the fourth step between the standard form of the stepped spillway and stepped spillway with TPEs of type A for the flow rate of 60 liters/second. Along the vertical surface from the step edge ($Z/h = 1$), the velocity increases until reaching a maximum value near the water surface. The location of the maximum velocity for model A-3 is about 0.83 cm above the step edge, and for other models of stepped spillways, the maximum velocity occurs about 1.17 cm above the step edge.

Figure 9(b)–9(e) compares the velocity distributions of different layouts of TPEs with the standard form of the stepped spillway. It can be seen that the implementation of TPEs led to a significant decrease in the flow velocity. Table 4 presents the velocity variations at two specified measurement points (with and without TPEs). Figure 9 and Table 5 show that models

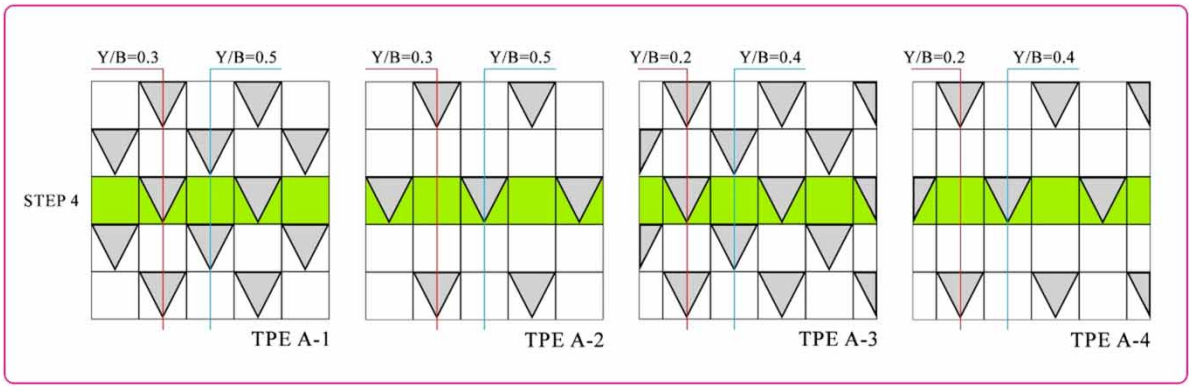

Figure 8 | Positions of measurement points to investigate the pressure and velocity distributions on the stepped spillway.

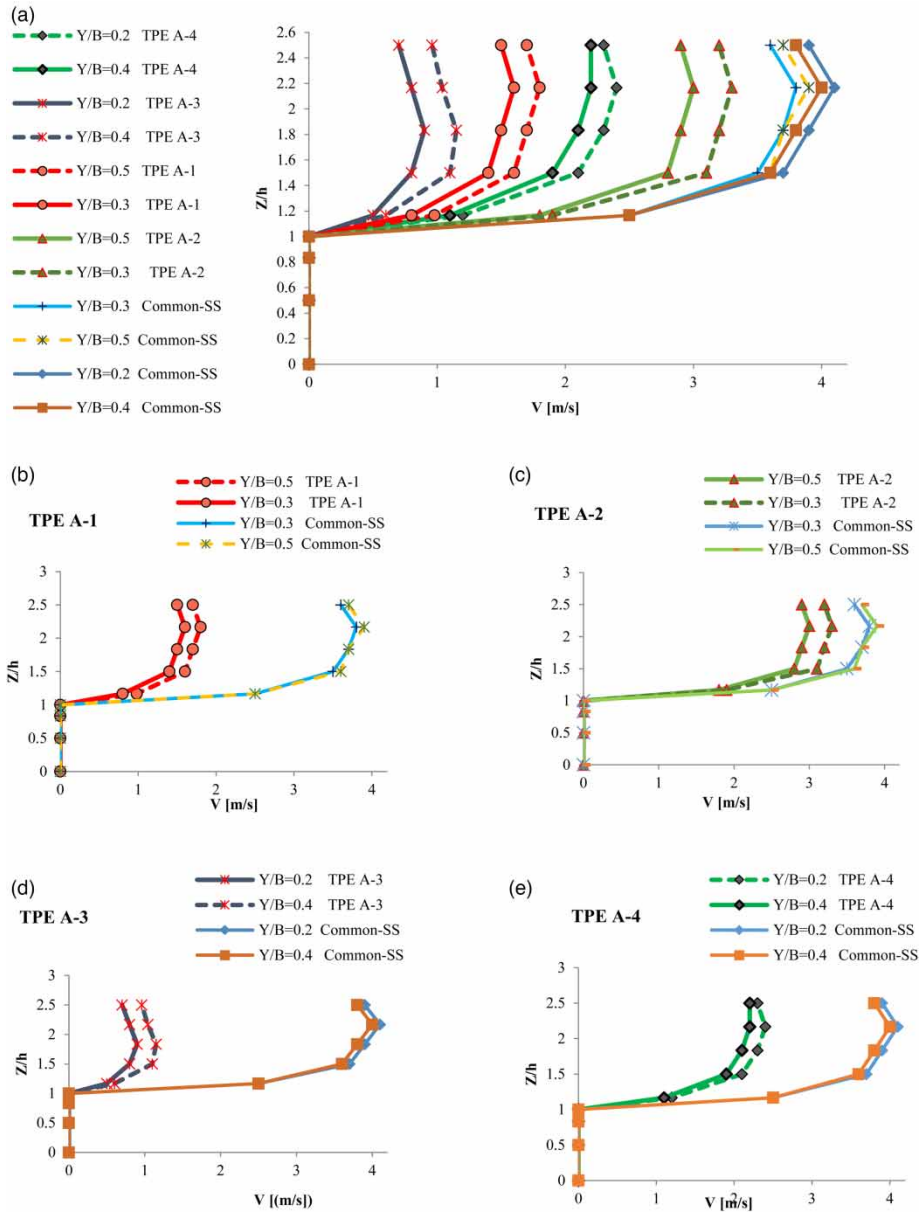

Figure 9 | Velocity distributions on the vertical surface of step number 4.

Table 5 | Velocity variations of stepped spillway with selected TPEs of type A

Stepped spillway with TPE	TPE A-1		TPE A-2		TPE A-3		TPE A-4	
Velocity variations (%)	$Y/B = 0.3$	$Y/B = 0.5$	$Y/B = 0.3$	$Y/B = 0.5$	$Y/B = 0.2$	$Y/B = 0.4$	$Y/B = 0.2$	$Y/B = 0.4$
	61	55	15	23	72	80	47	44

A-3, A-1, A-4, and A-2 show 72–80, 55–61, 44–47, and 15–23% reduction in velocities, respectively. This suggests that closer spacing of the elements leads to greater reductions in flow velocity. Moreover, the velocity reduction rate is slightly higher at a point with the prismatic element.

Figure 10 shows the numerical distribution of pressure over the standard form of the stepped spillway. The pressure reaches its minimum value on the upper part of the vertical surface of the steps, which can lead to a destructive cavitation phenomenon. Placing TPEs near the vertical surface of steps can reduce the flow velocity and prevent the cavitation phenomenon.

Figure 11(a) shows the pressure distribution on vertical surfaces of the fourth step. Along the vertical surface, the development of small eddies arises from the reverse flow inside the step cavity causing maximum pressure at the bottom. Negative pressures can be seen at $Z/h > 0.5$, and the minimum pressures occurred near the edge of the step. This pressure drop to the sub-atmospheric value is due to the flow detachment from the spillway surface. Note from Figure 11 that the minimum pressure on the vertical step surface of the common standard stepped spillway was 2–5 times larger than that of the stepped spillways with the TPEs. The pressure increased again at the step edge and then by passing through the region with a decreasing trend proportional to the flow depth reached to zero at the free surface. It is obvious that the pressure is zero from the

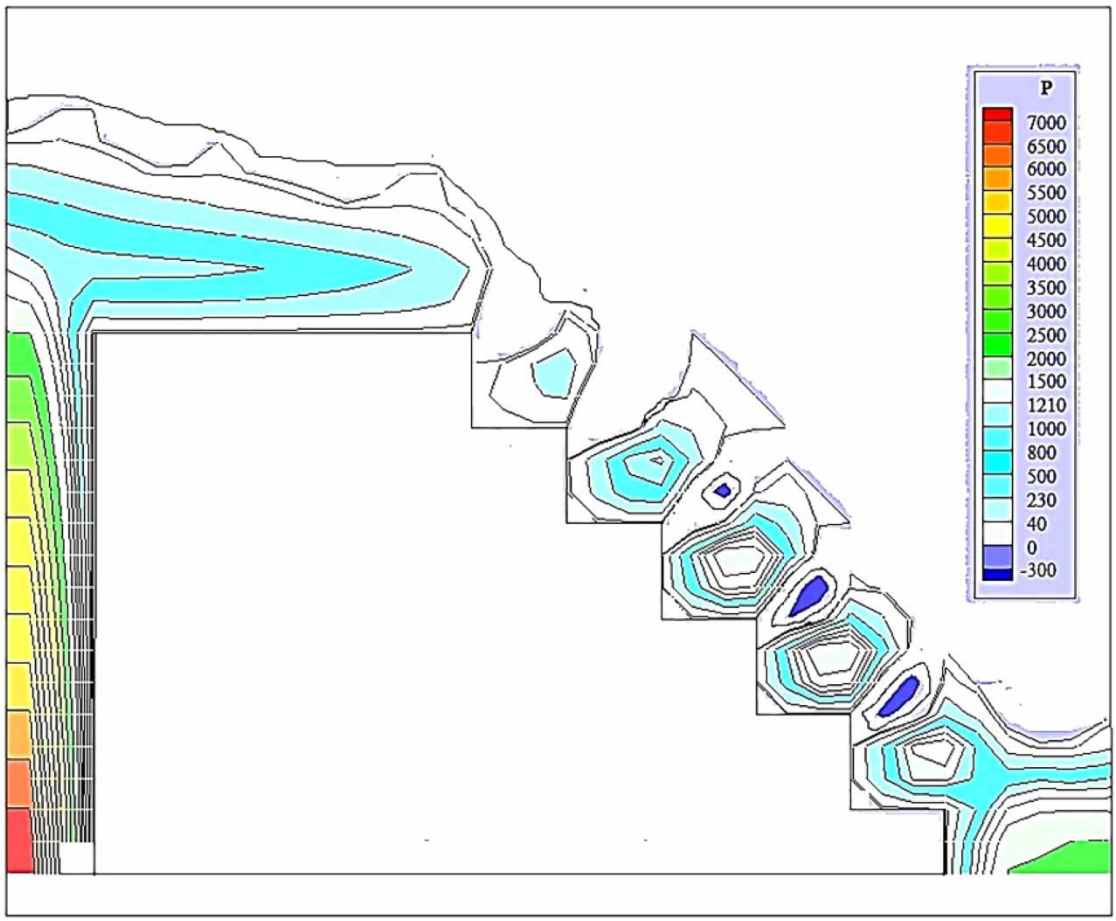

Figure 10 | Contour lines of the static pressure (Pa) for the standard form of the stepped spillway with discharge of 60 liters/second.

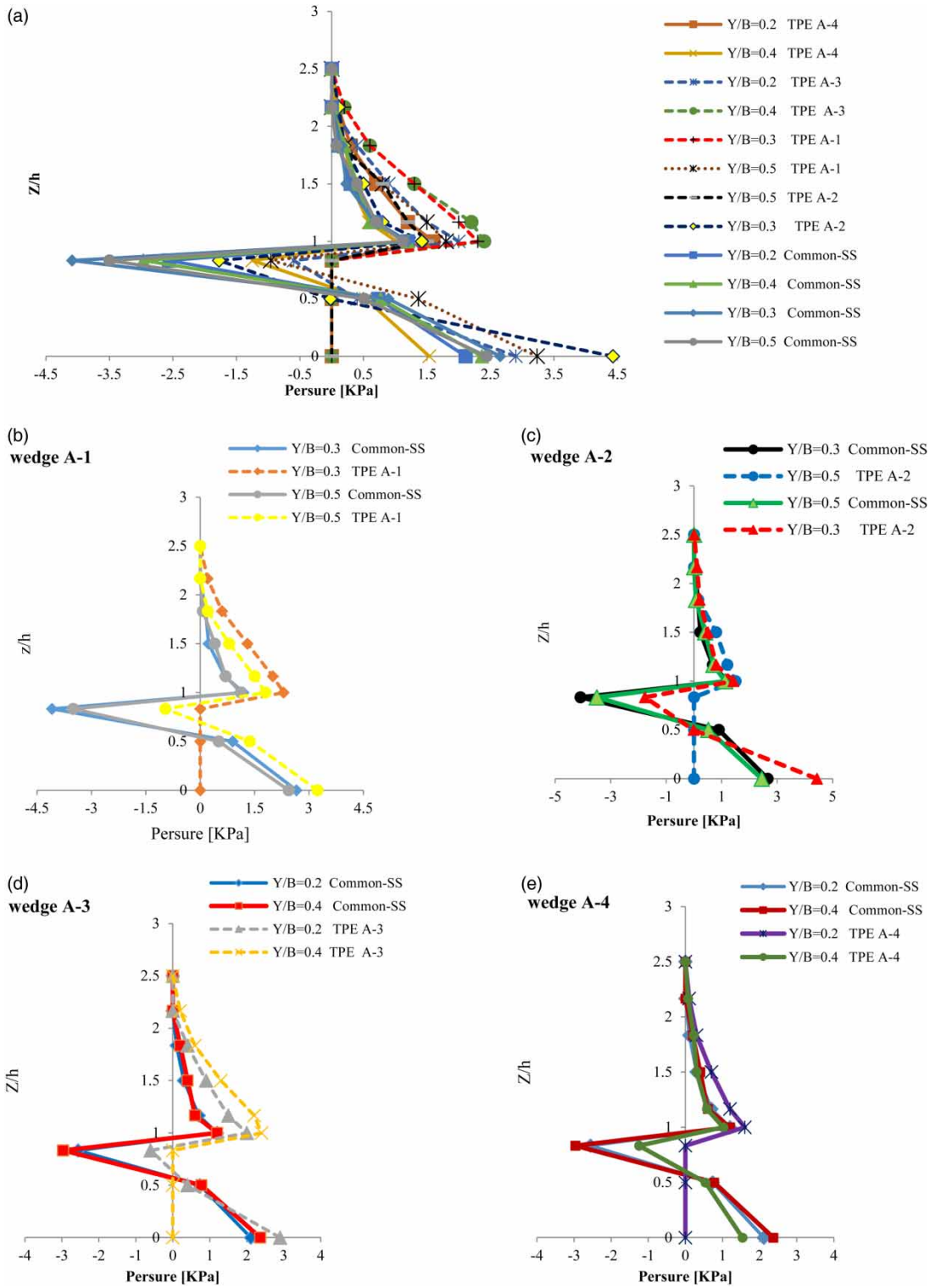

Figure 11 | Pressure distribution on the vertical surface of the fourth step.

bottom to the step edge ($Z/h = 1$) on measurement points where TPEs are placed for the stepped spillway with the prismatic element. Generally, as illustrated in Figure 11(b)–11(e), the pressure on the vertical step surface of the common standard stepped spillway reaches its maximum negative value at $Z/h = 0.83$ which can be significantly reduced by placing TPEs. The results also indicated that placing TPEs increases the positive pressure at the step edge ($Z/h = 1$).

Table 6 presents the variations of pressure at the step edge and vertical surface of step for the stepped spillway with effective TPEs of type A.

As seen in Table 6, adding TPEs with layouts of A-1, A-2, A-3, and A-4 can reduce the negative pressure on the vertical step surface by 72, 56, 96, and 59%, respectively. In addition, positive pressure in the step edge for models A-1, A-2, A-3, and A-4 increased by 93, 34, 200, and 37%, respectively. The decreasing and increasing trends of negative and positive pressures were striking when the elements were more densely spaced. These results suggest that models A-3, A-1, A-4, and A-2, respectively, showed the best performance in terms of reducing the cavitation damage potential.

Figure 12 shows the pressure distribution on the horizontal surface of the fourth step for different layouts of the type A prismatic element. In this figure, X represents the distance along the horizontal step face originating at the outer edge of the step, and L is the step length. It can be seen that the pressure on the horizontal step surface is distributed in a way that gives an approximately S-curve shape. Along the horizontal surface, the pressure decreased slightly, then it increased to the maximum value and decreased again near the step edge due to detachment of flow. The location of the maximum pressure in a standard stepped spillway and stepped spillway with layouts of A-4 and A-2 was about 0.7 apart from the step edge and for a stepped spillway with layouts of A-1 and A-3 was about 0.8 apart from the step edge. This maximum pressure is caused by the impact of the flow. Moreover, the minimum pressure occurred at $X/L = 0.2$ in all stepped spillways. By adding TPEs, the negative pressure near the corner of the step is converted to the positive pressure, which eliminates the risk of cavitation and increases the maximum pressure at the edge of the step. Models A-3, A-1, A-4, and A-2 showed the highest increase in the maximum and minimum pressures, respectively. Generally, the placement of TPEs on all steps with more density leads to better performance.

Figure 13 depicts the variations of the Darcy–Weisbach roughness coefficient (f) with various unit discharges for stepped spillways. Figure 13 shows that there is a considerable increase in roughness for the stepped spillway with TPEs. In addition, the TPEs of type A have greater effects on increasing the roughness coefficient than TPEs of type B.

Table 6 | Pressure variations of the stepped spillway with effective TPEs of type A

	TPE A-1		TPE A-2		TPE A-3		TPE A-4	
Stepped spillway with TPES	***Z/h* = 1**	***Z/h* = 0.83**	***Z/h* = 1**	***Z/h* = 0.83**	***Z/h* = 1**	***Z/h* = 0.83**	***Z/h* = 1**	***Z/h* = 0.83**
Variation of P (%)	+93	−72	+34	−56	+200	−96	+37	−59

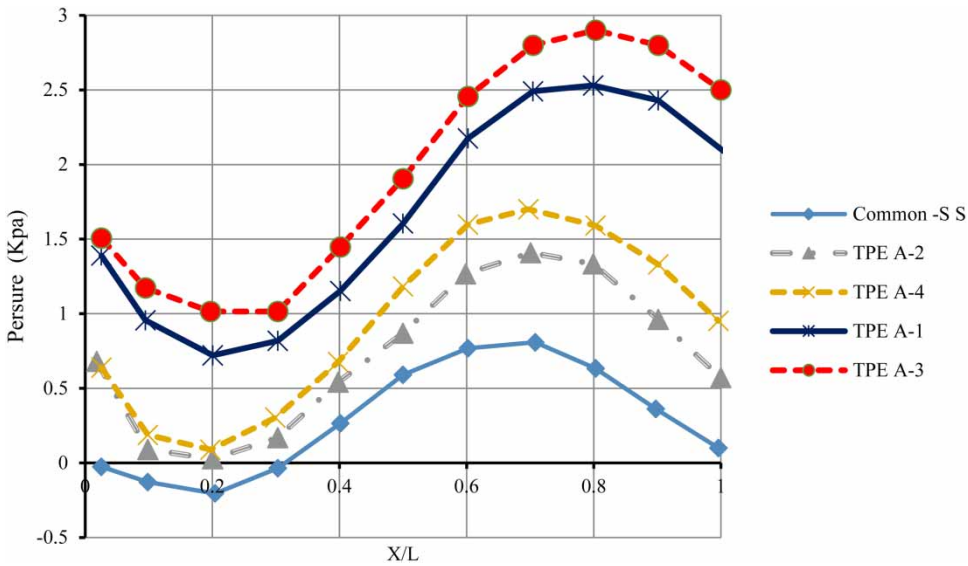

Figure 12 | Horizontal profile of the pressure distribution on the floor of step 4.

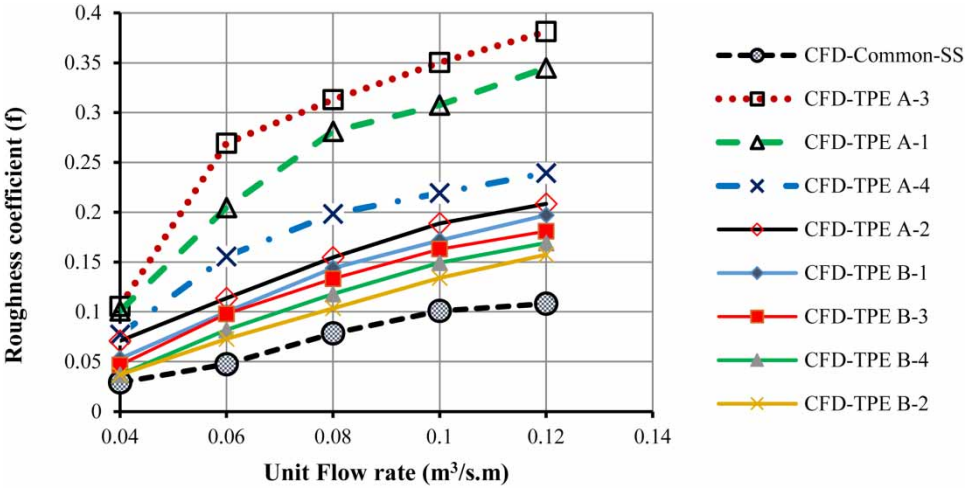

Figure 13 | Roughness coefficient changes with various unit discharges for stepped spillways.

Experimental study

Four effective models of stepped spillway TPEs (A-1, A-2, A-3, and A-4) with the best numerical performance were experimentally studied. In the present study, the critical depth (y_c), the primary depth of hydraulic jump (y_1), and the velocity at the spillway toe (V_1) were calculated using the measured discharge and the downstream sequent depth (y_2). In the last stage, The Darcy–Weisbach roughness coefficient is determined as follows (Henderson 1966):

$$f = \frac{8gq\sin\theta}{V_1^3} \tag{6}$$

The downstream sequent depth is illustrated in Figure 14 as a function of the unit discharge for stepped spillways. Regarding the MRE, it can be seen that the maximum difference for the standard stepped spillway was 4.6% and for the stepped spillway with layouts A-1, A2, A3, and A4 were 3.28, 3.02, 3.29, and 3.41%, respectively. One can conclude that there is a good agreement between the numerical and experimental results.

Figure 15 shows the energy dissipation rate changes with various unit discharges. It can be seen that the energy dissipation rates obtained by simulation and measurement are similar. It can be seen that the energy dissipation rates in stepped spillways with TPEs increase with an increase in the unit discharges and then decrease slightly. On the other hand, as the unit discharge

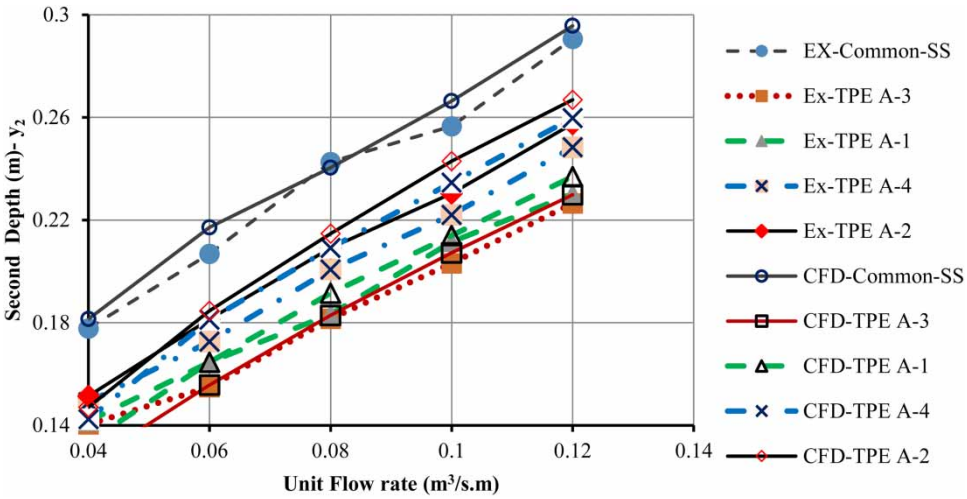

Figure 14 | Variations of sequent depth of downstream with various unit discharges for stepped spillways.

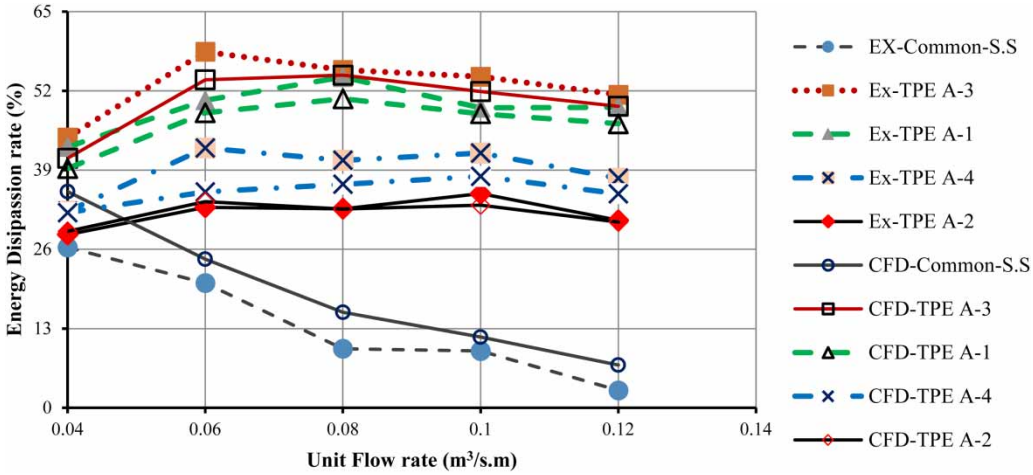

Figure 15 | Energy dissipation rate changes with various unit discharges for different stepped spillways.

increases, the rate of energy dissipation is reduced for the standard form of the stepped spillway. Furthermore, comparing the performance of the different stepped spillways showed that the energy loss in the stepped spillway with TPEs is greater. Energy dissipation for TPEs A-1, A-2, A-3, and A-4 is increased by 2.4, 1.24, 2.7, and 1.62 times, respectively, compared to the standard stepped spillway. Generally, it can be stated that installing TPEs increases the roughness of steps and dissipates more energy. Moreover, as can be inferred from the numerical and experimental results, for a given unit discharge with increasing elements densities, the energy dissipation increases. Stepped spillways with layouts of A-1 to A-4 perform the best in terms of energy dissipation.

In Figure 16, the Darcy–Weisbach roughness coefficient (f) is depicted as a function of the critical depth to the step roughness ratio (y_c/K). As seen in this figure, as the ratio of yc/K increases, the roughness coefficient (f) increases. It is clear that the roughness coefficient (f) increases with a denser spacing of TPEs. This relative increase for different layouts of TPEs varies between 20 and 47%.

CONCLUSIONS

To develop an improved understanding of energy dissipation provided by stepped spillways with TPEs, two types of TPEs with different layouts were tested numerically. Based on the results of numerical simulation, stepped spillways with the TPEs of type A provided higher roughness coefficient, lower downstream sequent depth, and consequently, higher energy dissipation compared to the standard stepped spillway and stepped spillway with TPEs of type B. It was also concluded

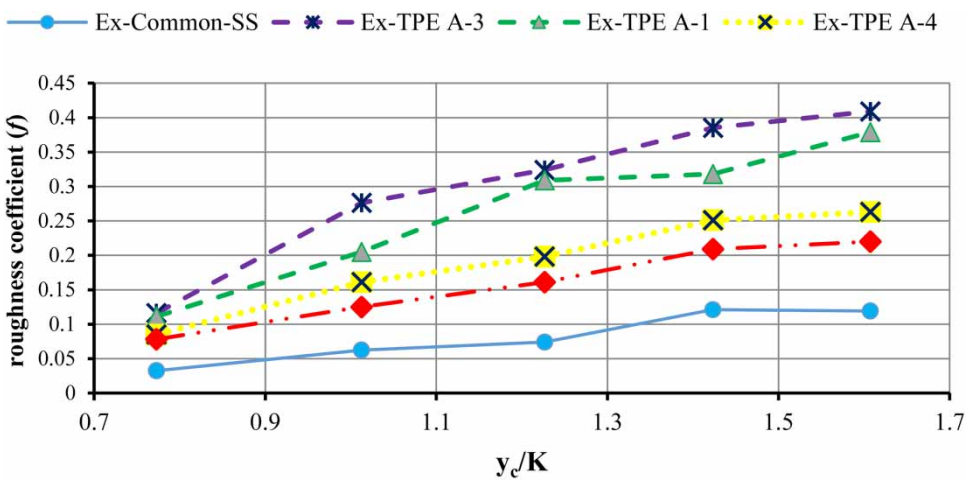

Figure 16 | Roughness coefficients (f) versus the critical depth to the step roughness ratio (y_c/K).

that the denser TPEs, the better the performance. In fact, with closer spacing of the TPEs, the downstream sequent depth decreased by 13–21%, roughness coefficient (f) increased by 20–47%, and as a result, energy dissipation increased by 1.24–2.7 times. The detailed conclusions are drawn.

Velocity profiles indicated that models A-3, A-1, A-4, and A-2 can decrease the vertical surface velocity by 72–80, 55–61, 44–47, and 15–23%, respectively. Implementing TPEs is an effective way to decrease negative pressures and prevent cavitation phenomena. Results showed that models A-3, A-1, A-4, and A-2 decrease negative pressures on the vertical face by 96, 72, 59, and 56%, respectively, and increase positive pressures on the step edge by 200, 93, 37, and 34%, respectively. The present study will serve little purpose unless a definite improvement in cost can be shown, as most spillways for dams are safe against excessive scour. The constructability of the proposed TPEs must also be easy to avoid time delays for roller compacted concrete (RCC) placement.

The following methods to construct these TPEs are proposed:

- Develop a special shutter and cast the TPEs with skin concrete together with normal RCC placement.
- Precast the TPEs, lift the elements with a mobile crane to the desired position, dowel them into the downstream steps, and grout the contact.
- Precast a mass element that will also be used as a 'permanent shutter'.

An important issue in using the proposed elements is the additional cost. Two main cost additions are relevant: the extra amount of concrete required and the increase in the shutter length, depending on which of the above-mentioned methods is used. The cost estimate shows a small increase in the total cost of the spillway. However, the cost/scour benefit must be qualified to determine if the addition of TPEs is worth the effort. These explanations were added in the conclusion section.

DATA AVAILABILITY STATEMENT

All relevant data are included in the paper or its Supplementary Information.

REFERENCES

Abbasi, S. & Kamanbedast, A. A. 2012 Investigation of effect of changes in dimension and hydraulic of stepped spillways for maximization energy dissipation. *World Applied Sciences Journal* **18** (2), 261–267.

Arjenaki, M. O. & Sanayei, H. R. Z. 2020 Numerical investigation of energy dissipation rate in stepped spillways with lateral slopes using experimental model development approach. *Modeling Earth Systems and Environment* **6** (2), 1–12.

Attarian, A., Hosseini, K., Abdi, H. & Hosseini, M. 2014 The effect of the step height on energy dissipation in stepped spillways using numerical simulation. *Arabian Journal for Science and Engineering* **39** (4), 2587–2594.

Azhdary Moghaddam, M. 1997 *The Hydraulics of Flow on Stepped Ogee-Profile Spillways*. Doctoral Dissertation, University of Ottawa, Canada.

Bakhtyar, R. & Barry, D. A. 2009 Optimization of cascade stilling basins using GA and PSO approaches. *Journal of Hydroinformatics* **11** (2), 119–132.

Barani, G. A., Rahnama, M. B. & Sohrabipoor, N. 2005 Investigation of flow energy dissipation over different stepped spillways. *American Journal of Applied Sciences* **2** (6), 1101–1105.

Boes, R. M. & Hager, W. H. 2003 Hydraulic design of stepped spillways. *Journal of Hydraulic Engineering* **129** (9), 671–679.

Chamani, M. R. & Rajaratnam, N. 1994 Jet flow on stepped spillways. *Journal of Hydraulic Engineering* **120** (2), 254–259.

Chanson, H. 1994 Comparison of energy dissipation between nappe and skimming flow regimes on stepped chutes. *Journal of Hydraulic Research* **32** (2), 213–218.

Felder, S., Guenther, P. & Chanson, H. 2012 *Air-Water Flow Properties and Energy Dissipation on Stepped Spillways: A Physical Study of Several Pooled Stepped Configurations.* No. CH87/12. School of Civil Engineering, The University of Queensland, Brisbane.

Harlow, F. H. & Nakayama, P. I. 1968 *Transport of Turbulence Energy Decay Rate*. No. LA-3854. Los Alamos Scientific Lab, N. Mex.

Hekmatzadeh, A. A., Papari, S. & Amiri, S. M. 2018 Investigation of energy dissipation on various configurations of stepped spillways considering several RANS turbulence models. *Iranian Journal of Science and Technology, Transactions of Civil Engineering* **42** (2), 97–109.

Henderson, F. M. 1966 *Open Channel Flow*. MacMillan Company, New York.

Kavian Pour, M. R. & Masoumi, H. R. 2008 New approach for estimating of energy dissipation over stepped spillways. *International Journal of Civil Engineering* **6** (3), 230–237.

Li, S., Li, Q. & Yang, J. 2019 CFD modelling of a stepped spillway with various step layouts. *Mathematical Problems in Engineering* **2019**, 6215739.

Li, S., Yang, J. & Li, Q. 2020 Numerical modelling of air-water flows over a stepped spillway with chamfers and cavity blockages. *KSCE Journal of Civil Engineering* **24** (1), 99–109.

Moghadam, M. K., Amini, A. & Moghadam, E. K. 2020 Numerical study of energy dissipation and block barriers in stepped spillways. *Journal of Hydroinformatics* **23** (2), 284–297.

Morovati, K., Eghbalzadeh, A. & Javan, M. 2016 Numerical investigation of the configuration of the pools on the flow pattern passing over pooled stepped spillway in skimming flow regime. *Acta Mechanic Journal* **227**, 353–366.

Parsaie, A. & Haghiabi, A. H. 2019 The hydraulic investigation of circular crested stepped spillway. *Flow Measurement and Instrumentation* **70**, 101624.

Peng, Y., Zhang, X., Yuan, H., Li, X., Xie, C., Yang, S. & Bai, Z. 2019 Energy dissipation in stepped spillways with different horizontal face angles. *Energies* **12** (23), 4469.

Roushangar, K., Foroudi, A. & Saneie, M. 2019 Influential parameters on submerged discharge capacity of converging ogee spillways based on experimental study and machine learning-based modeling. *Journal of Hydroinformatics* **21** (3), 474–492.

Sarkardeh, H., Marosi, M. & Roshan, R. 2015 Stepped spillway optimization through numerical and physical modeling. *International Journal of Energy and Environment* **6** (6), 597.

Shahheydari, H., Nodoshan, E. J., Barati, R. & Moghadam, M. A. 2015 Discharge coefficient and energy dissipation over stepped spillway under skimming flow regime. *KSCE Journal of Civil Engineering* **19** (4), 1174–1182.

Tabari, M. M. R. & Tavakoli, S. 2016 Effects of stepped spillway geometry on flow pattern and energy dissipation. *Arabian Journal for Science and Engineering* **41** (4), 1215–1224.

Toombes, L. & Chanson, H. 2000 Air-water flow and gas transfer at aeration cascades: a comparative study of smooth and stepped chutes. In *Proceedings of the International Workshop on Hydraulics of Stepped Spillways*, Zurich, Switzerland, pp. 22–24.

Torabi, H., Parsaie, A., Yonesi, H. & Mozafari, E. 2018 Energy dissipation on rough stepped spillways. *Iranian Journal of Science and Technology, Transactions of Civil Engineering* **42** (3), 325–330.

Wüthrich, D. & Chanson, H. 2014 Hydraulics, air entrainment, and energy dissipation on a Gabion stepped weir. *Journal of Hydraulic Engineering* **140** (9), 04014046.

Yakhot, V. & Orszag, S. A. 1986 Renormalization group analysis of turbulence. I. Basic theory. *Journal of Scientific Computing* **1** (1), 3–51.

Yakhot, V. & Smith, L. M. 1992 The renormalization group, the ε-expansion and derivation of turbulence models. *Journal of Scientific Computing* **7** (1), 35–61.

First received 28 February 2021; accepted in revised form 21 January 2022. Available online 8 February 2022